Subtle Fluorination of Conjugated Molecules Enables Stable Nanoscale Assemblies on Metal Surfaces

Jens Niederhausen,[†,‡,§] Yuan Zhang,[†] Fairoja Cheenicode Kabeer,[‖] Yves Garmshausen,[⊥]
Bernd M. Schmidt,[#] Yang Li,[†] Kai-Felix Braun,[†] Stefan Hecht,[⊥] Alexandre Tkatchenko,[‖,¶]
Norbert Koch,*[,‡,§] and Saw-Wai Hla*[,†,∇]

[†]Nanoscale and Quantum Phenomena Institute, Physics & Astronomy Department, Ohio University, Athens, Ohio 45701, United States

[‡]Institut für Physik & IRIS Adlershof and [⊥]Institut für Chemie & IRIS Adlershof, Humboldt-Universität zu Berlin, 12489 Berlin, Germany

[§]Helmholtz-Zentrum Berlin für Materialien und Energie GmbH, 12489 Berlin, Germany

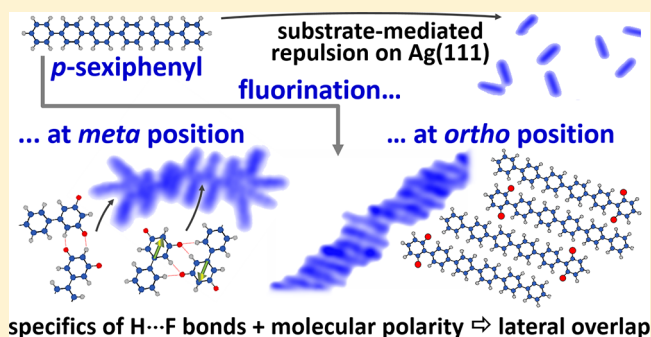[‖]Fritz-Haber-Institut der Max-Planck-Gesellschaft, 14195 Berlin, Germany

[#]Institute of Organic and Macromolecular Chemistry, Heinrich-Heine-University Düsseldorf, 40225 Düsseldorf, Germany

[¶]Physics and Materials Science Research Unit, University of Luxembourg, L-1511 Luxembourg, Luxembourg

[∇]Center for Nanoscale Materials, Argonne National Laboratory, Argonne, Illinois 60439, United States

ⓢ Supporting Information

ABSTRACT: In molecular self-assembly on surfaces, the structure is governed by the intricate balance of attractive and repulsive forces between molecules as well as between molecules and the substrate. Frequently, repulsive interactions between molecules adsorbed on a metal surface dominate in the low-coverage regime, and dense self-assembled structures can only be observed close to full monolayer coverage. Here, we demonstrate that fluorination at selected positions of conjugated molecules provides for sufficiently strong, yet nonrigid, H···F bonding capability that (i) enables the formation of stable nanoscale molecular assemblies on a metal surface and (ii) steers the assemblies' structure. This approach should be generally applicable and will facilitate the construction and study of individual nanoscale molecular assemblies with structures that are not attainable in the high-coverage regime.

p-sexiphenyl → substrate-mediated repulsion on Ag(111)

fluorination…

… at *meta* position — … at *ortho* position

specifics of H···F bonds + molecular polarity ⇨ lateral overlap

INTRODUCTION

Molecular self-assembly is recognized as a key process in the formation of functional structures from the nano- to macro-scale in biology, chemistry, and physics.[1−5] By exploiting the interplay of noncovalent interactions, complex and stable arrangements can be formed with a minimal input of energy. The simultaneous action of attractive and repulsive forces cover a wide range of stabilizing and destabilizing energy values, from a few meV to several 100 meV.[6] When selecting the appropriate magnitude for each intermolecular force in the target structure, the thermal energy at room temperature (ca. 26 meV) can provide for sufficient dynamics that enables efficient self-assembly and allows self-healing or adaptiveness to the environment of the molecular assembly.[7]

In the fields of organic and molecular electronics, the self-assembly building blocks are predominantly π-conjugated molecules. By nature, these comprise intramolecular polar bonds. Therefore, electrostatic dipole and multipole inter-actions play an important role in structure formation.[8,9]

Likewise, hydrogen bonds can be a dominant factor in molecular self-assembly.[10,11] In addition to these interactions of permanent charges, mutual polarization and dispersion interactions contribute substantially. All of these are partic-ularly important for molecules on solid surfaces such as metals, as the pairwise interaction magnitude may vary considerably for molecule−molecule and molecule−substrate.[12,13] Yet, predicting the self-assembled structure for a given material combination, based on a known molecular and substrate structure, remains one of the major challenges, as a reliable hierarchical ranking of the governing interaction energies based on empirical knowledge is not sufficiently possible.

In this contribution, we study the structure of assemblies formed by three conjugated molecules with very similar chemical structure, differing only by two fluorine atoms and
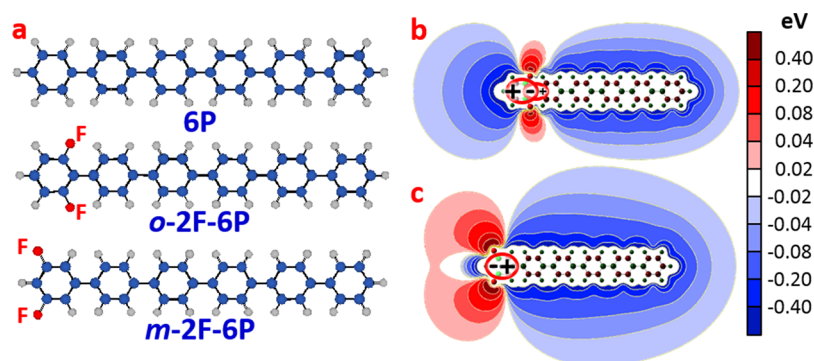
Figure 1. Employed molecules. (a) Chemical structure of 6P, *m*-2F-6P, and *o*-2F-6P. (b,c) Electrostatic potential maps of *o*-2F-6P and *m*-2F-6P, respectively.

the associated molecular dipole moment, on an Ag(111) surface. Scanning tunneling microscopy (STM) evidences that the self-assembled structures differ substantially, but attempts to explain these based on plausible consideration of the dominant interactions, dipole−dipole and fluorine-mediated hydrogen bonding, have failed. Only with state-of-the-art density functional theory (DFT) modeling and deliberate discrimination of all involved interactions, that is, electrostatic due to permanent charges, polarization and dispersion, as well as hydrogen bonding, we can fully rationalize the experimental findings and provide new insight for advanced self-assembly strategies. Our results underline the importance of very careful molecular design as numerous interaction parameters are correlated and also demonstrate the distinctive power of modern DFT methods, developed only very recently, to provide an understanding of fairly large and complex systems.

One approach to influence the structure of a molecular assembly is the introduction of a dipole in an otherwise nondipolar molecule to exploit dipole−dipole interaction. Frequently, this is achieved by replacing the peripheral hydrogen of a conjugated molecule by electron-withdrawing fluorine. A prototypical example that we consider here is *para*-sexiphenyl (6P)[14−20] and two partially fluorinated derivatives (see Figure 1a for chemical structures). For *o*-2F-6P, two fluorine atoms are placed in both ortho positions of the terminal benzene ring (relative to the phenyl−phenyl connection), and for *m*-2F-6P, in both meta positions. The two highly polar C−F bonds in each molecule result in dipoles along the long axis, with opposite direction for the two molecules. However, this is already a simplistic view of the net-dipole creating charge-density patterns. In the meta position, the electron density is accumulated at the outward-directed fluorine atoms with negligible charge transfer from the neighboring benzene ring, yielding an electric dipole of 2.2 D in the gas phase (Figure 1b). By contrast, for ortho substitution, also the neighboring benzene ring contributes to the electron density accumulated at the fluorine atoms. This charge pattern can be viewed as two electric dipoles opposing each other, however, with different magnitude, yielding a smaller net-dipole moment of 1.1 D (Figure 1c). These rather subtle differences already make it less obvious how the molecules would arrange on a metal surface. In addition, fluoroaromatics can feature H···F hydrogen bonding, whose stabilizing energy can vary vastly.[21−26] In fact, replacement of hydrogen atoms by fluorine atoms has been shown to result in substantial changes in the bulk structure of conjugated

molecules and polymers, with considerable impact on optical and charge-transport properties.[27−32]

■ METHODS

General Synthetic and Analytical Methods. The intermediate building block 1-(4-bromophenyl)-4-(biphenyl-4-yl)-1,4-bis(methoxymethyloxy)cyclohexane was described in a previous study.[33] The syntheses of additional building blocks, 3,5-difluoro-4′-(4,4,5,5-tetramethyl-1,3,2-dioxaborolan-2-yl)-biphenyl and 3,5-difluorobiphenyl-4′-boronic acid, as well as the final products, *o*-2F-6P and *m*-2F-6P, are described in the Supporting Information. [1]H and ^{13}C nuclear magnetic resonance (NMR) spectra of intermediates and precursors can also be found there.

Low-Temperature STM. The experiments were performed by using a custom-built ultrahigh vacuum (STM) system.[34] A single-crystal Ag(111) substrate was cleaned by repeated cycles of sputtering with Ne ions followed by annealing to 700 K. For a comparative study, 6P and the two types of fluorinated 6P molecules were stepwise deposited separately by using the same deposition parameters from a custom-built Knudsen cell onto an Ag(111) substrate via thermal evaporation. For all three molecules we performed depositions with the sample at room temperature. 6P and *m*-2F-6P were additionally deposited with the sample at a temperature of ca. 70 K. For *m*-2F-6P, a post-deposition annealing was carried out. Possibly, the grain size and/or length of the supramolecular chains is influenced by the preparation conditions. However, such a quantitative analysis was prevented in the current experiments by the tip−molecule interaction that gave rise to frequent but random destruction of the molecular arrangements. After each deposition, the sample was transferred to the STM chamber in situ and cooled down to ≈6 K for the experiments. All presented images are representative for the respective molecular films as deduced from multiple film preparations and tens of different investigated spots per system.

A Gaussian or low-pass filter were applied to some STM images to reduce the noise level. Some images are presented as rendered three-dimensional (3D) view, as indicated in the figure caption.

First-Principles Electronic Structure Calculations. First-principles electronic structure calculations employed the DFT code FHI-aims[35] to investigate the self-assembly of 6P molecules and fluorinated 6P derivatives adsorbed on the Ag(111) surface. To account for van der Waals (vdW) interactions, calculations have been performed with either the DFT + vdW method[36,37] or the DFT + many-body dispersion

(MBD) method.[38] The DFT + vdW method combines the Tkatchenko—Scheffler (TS) DFT + vdW[36] method for intermolecular interactions with the Lifshitz—Zaremba—Kohn theory,[36,39] including the collective response of the substrate electrons in the calculation of the molecule-surface vdW energy. The DFT + MBD method in addition includes many-body contributions to the vdW dispersion energy for both molecule-surface and molecule—molecule interactions.[38,40] Throughout this work, we employ the Perdew—Burke—Ernzerhof[41] (PBE) functional with converged settings for the integration grids and standard numerical atom-centered orbital basis sets. The atomic zeroth-order regular approximation[42] was used to treat the relativistic effects for all atoms. A silver slab with a 20×8 surface cell and four metal layers was used throughout. We used a Monkhorst—Pack grid of $1 \times 1 \times 1$ k-points.[43]

We calculated the total energy for 6P dimer and fluorinated 6P dimer structures in the gas phase and on the Ag(111) surface, including dispersion interactions, with both the DFT + vdW and DFT + MBD methods. The calculations were carried out for different stacking of the dimers, as shown in Figure 5, with the inter-ring twist angle set to $\approx 11.4°$.[18] The long molecular axes of the two molecules in the dimer structures are separated by ≈ 7.0 Å,[20] resulting in a H···F contact length of ca. 2.6 Å. For the structures including the Ag surface, the molecules are located ≈ 3.0 Å from the topmost metallic layer[44,45] and are aligned along the Ag[110] direction. A visualization of the on-surface structures can be found in Figure S2.

Dimer structures were not further optimized, but we tested the difference between relaxed and single-point calculations. As reported in Table S1, only the total energies differ notably, whereas the absolute binding energies, vdW contribution, and Hirshfeld charge transfer are comparable. Note that we report only relative binding energies in the manuscript. For these, the difference between the relaxed and single-point calculations is significantly reduced compared to the absolute values.

X-ray Diffraction. To test the ability of our molecules in forming H···F hydrogen bonds, we attempted to grow single crystals. Sexiphenyls used herein are generally arduous to crystallize because of their low symmetry. We took great effort and succeeded in crystallizing a suitable model compound, *m*-4F-6P,[27] by sublimation in a custom-made apparatus[46] at high temperature over several days. All tested crystals showed twinning phenomena, which could be solved for one particularly good crystal, and the data are presented in the Supporting Information.

■ RESULTS AND DISCUSSION

Although the changes in the chemical structure of these three molecules may seem small, the self-assembled structures on Ag(111) in the submonolayer and monolayer regimes are huge. For the nondipolar 6P, we find individually adsorbed molecules at low and medium coverages (see STM images in Figure 2), and only when approaching monolayer coverage, we find the formation of rows of uniform width formed by densely packed molecules with the long molecular axis perpendicular to the row direction (see Figure S21).

For *o*-2F-6P, we find only very few individual molecules on the surface. Most molecules assemble in rows, as those shown in Figure 3. The two consecutively taken images shown as insets of Figure 3a evidence that the molecules stay closely packed even when moved away from the row by the STM tip.
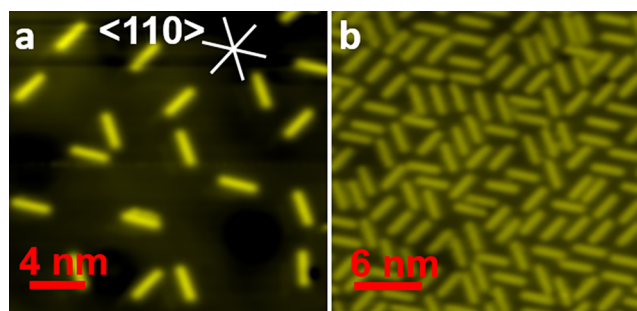

Figure 2. 6P structures. STM image of individual 6P molecules on Ag(111) at (a) low and (b) medium coverages. The molecules are mostly oriented with their long molecular axis along [110] and equivalent directions of the surface [a: $V = -2$ V, $I = 0.1$ nA, 23.1 nm $\times$ 22 nm scan; b: 2 V, $I = 27$ pA 28.1 nm $\times$ 26.8 nm scan].

In contrast to the 6P rows at high coverage, the *o*-2F-6P long molecular axes are not perfectly perpendicular to the row direction (indicated by the red arrows and white dashed lines in Figure 3a), and the edges of each row appear fringed, that is, subsequent molecules are typically laterally displaced by a stack-shift of one or two benzene rings with respect to the side-by-side arrangement found for 6P. For a single *o*-2F-6P molecule, one end of the molecule appears brighter in STM imaging, which we attribute to the fluorine-bearing terminal benzene ring (indicated by the green arrow in Figure 3b). The apparent height line profiles across 12 consecutive molecules within a row, as indicated by the alternating green and blue lines in Figure 3b, are shown in Figure 3c after removal of the stack-shift. This evaluation reveals alternating left and right higher ends of the molecules, evidencing that the molecular dipoles are positioned in an antiparallel arrangement. With the proper molecular orientation at hand, the STM image in Figure 3b was partially overlaid with *o*-2F-6P representations, illustrating that mostly more than two and routinely five benzene rings separate the dipole-bearing terminal rings of two adjacent molecules. Notably, for the latter configuration, the ring that carries the proton acceptor for hypothetical H···F hydrogen bond formation is overlapping with only one neighboring molecule.

Finally, the structure formed by *m*-2F-6P differs distinctly from the former two. A line profile analysis like the one in Figure 3c also yielded antiparallel adjacent molecules (cf. Figure S24). However, the stack-shift between subsequent molecules is huge, very often five benzene rings, resulting in the apparent "zipper" structure seen in Figure 4. In some instances, deviations from this zipper configuration are observed. For instance, the green arrows in Figure 4a indicate such regions where neighboring molecules have a smaller stack-shift. Similar to the case of *o*-2F-6P, and indicated by the red arrow and white dashed lines in Figure 4a, such regions give rise to a significant discrepancy between the orthogonal of the long molecular axes and the long-range stacking direction. As for *o*-2F-6P and 6P rows at high coverage, the distance between subsequent molecules is 0.7 nm. This was shown in a previous STM study to correspond to flat-on adsorbed molecules, whereas a distance of 0.4 nm would be tantamount for an edge-on adsorption geometry.[20] At the end of the rows, we often find a "canted" arrangement of *m*-2F-6P with angles of ca. 60° between the molecular axes, thus forming a "starlike" end of a row. As the side-by-side arrangement allows for the maximum dipole—dipole effect and, in view of the extreme
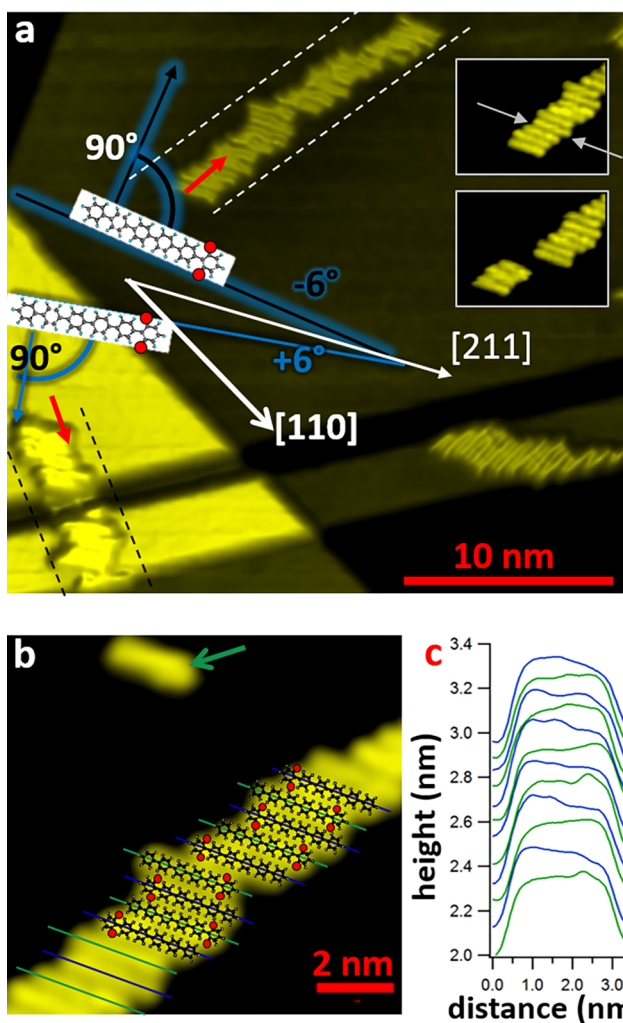
Figure 3. *o*-2F-6P structures. (a) Large-area STM image showing three self-assembled rows of *o*-2F-6P molecules. The bottom two rows exhibit a "carpet mode" where the molecules within a row cross over the surface steps and troughs. This indicates that the molecule–molecule interaction is sufficiently strong to overcome step-barriers. The molecular alignment and average stacking direction are indicated [*V* = −1.5 V, *I* = 0.1 nA, 30 nm × 28 nm scan, 3D view]. Inset: Two consecutively acquired images that evidence the STM scan-induced detachment of three hydrogen-bonded molecules at the indicated position [*V* = −1.5 V, *I* = 0.1 nA, 9.8 nm × 7.3 nm scan]. (b) Molecules form a stack arrangement with lateral shifts along the row. A single molecule appears with a bright end indicated with an arrow [*V* = −1.5 V, *I* = 0.1 nA, 11.4 nm × 11.1 nm scan]. (c) A sequence of line profiles of 12 consecutive molecules in (b) show higher heights at either right (green) or left (blue) ends.

polarizability asymmetry of rodlike molecules, also gives rise to the largest dipole-induced dipole effect, the observation of the canted arrangements is first evidence that the molecular dipole moment by itself does not dominate the structures.

The fact that we find individual 6P molecules on Ag(111) and, instead, molecular aggregates for the fluorinated ones at low coverage indicates that repulsive interactions dominate between 6Ps, whereas net attractive forces persist for adsorbed *o*-2F-6P and *m*-2F-6P molecules. At first sight, the interaction of molecular dipoles and H···F hydrogen bonds would appear as candidates facilitating aggregate formation.

However, without further insight, it remains elusive why apparently both interactions dictate the structure for *m*-2F-6P
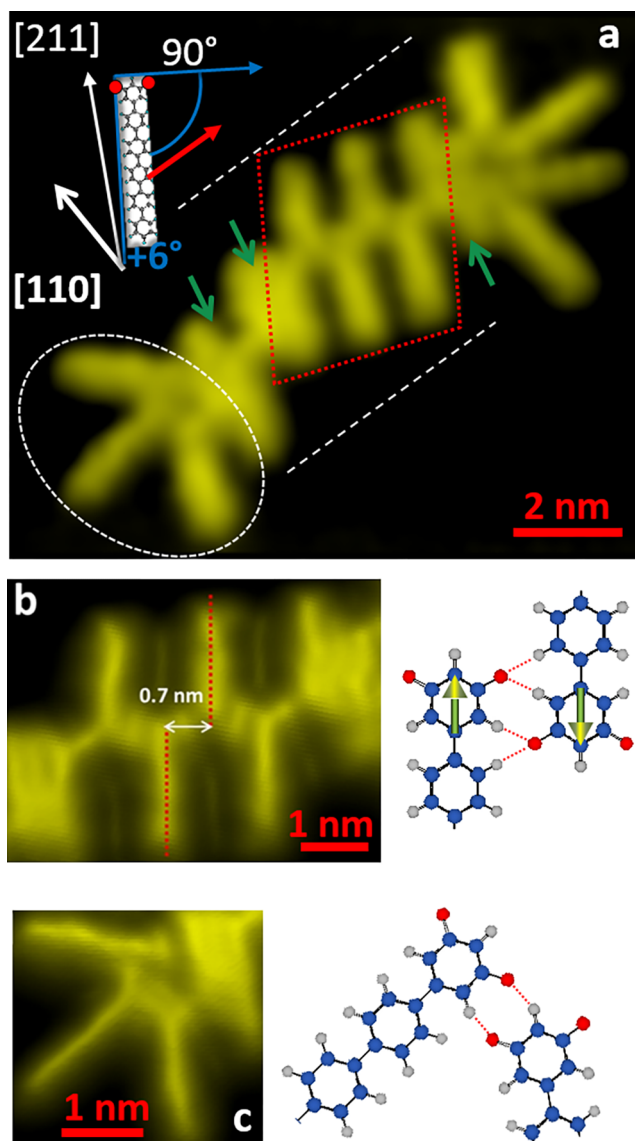

Figure 4. *m*-2F-6P structures. (a) STM image of *m*-2F-6P rows showing zipper (red dotted parallelogram) and canted (white dashed oval) arrangements. The green arrows indicate more densely packed local structures. The molecular alignment and average stacking direction are indicated [*V* = −1 V, *I* = 0.1 nA, 15.3 nm × 9.4 nm scan]. (b) A zoom of a zipper arrangement [*V* = −1 V, *I* = 0.1 nA, 3D view]. The measured distance between the neighboring molecules is 0.7 nm. The corresponding schematic shows the antiparallel dipole configuration and H···F bonding sites. (c) STM image of a canted arrangement [*V* = −1 V, *I* = 0.1 nA, 3D view]. The corresponding schematic shows H···F bonding sites. Because the canted arrangement facilitates a "turnaround" of the supramolecular chain, it allows *all* fluorine atoms to feature an H···F bond.

(immediate proximity of molecular dipoles and possibly two H···F bonds per molecule); but for *o*-2F-6P the dipoles are generally rather separated in space and a configuration with seemingly nonoptimal stack-shift for two H···F bond formations persists. Furthermore, the molecular packing density varies significantly in the different row arrangements, so that stabilizing polarization and dispersion interactions vary substantially as well.

To gain the required insight, we investigate the binding energy of molecular dimers as a function of the lateral shift

between them, that is, the stack-shift, with DFT using the PBE functional. One of the molecules is kept in a fixed position, while the other molecule is shifted, one ring at a time, along the long molecular axis direction. The nomenclature, shown in Figure 5, is such that configuration (5) corresponds to a side-
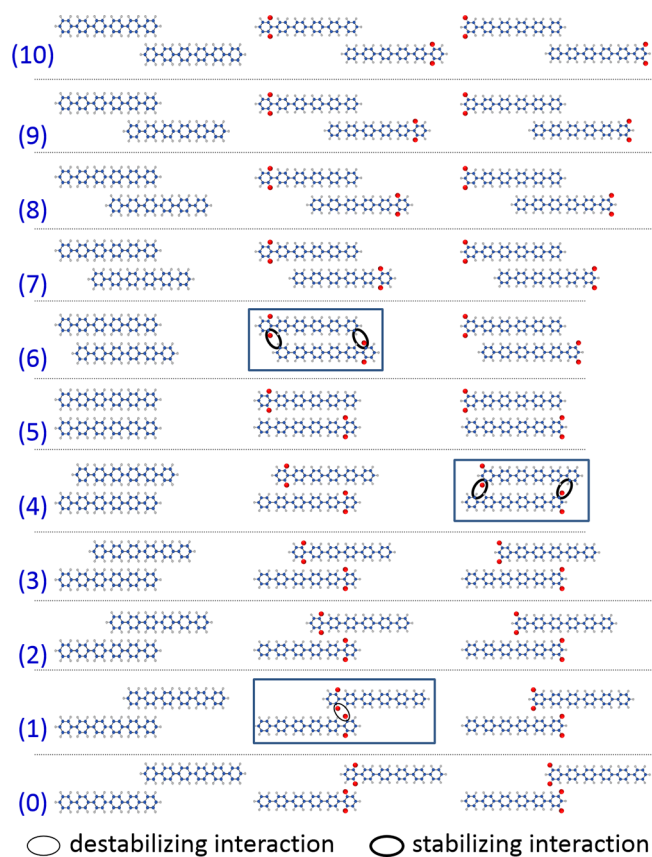

Figure 5. Dimer structures used for the calculations. The boxes indicate configurations that highlight specific interactions (encircled) between rings that are not direct neighbors, as discussed in the main text. The intermolecular F to F contact in the oval with thin line amounts to 2.9 Å.

by-side arrangement and configurations (0) and (10) both exhibit a stack-shift of five rings. In configuration (0), the o-2F-6P and m-2F-6P dimers have the fluorine-bearing rings located

next to each other, whereas in configuration (10) their separation is maximal. Furthermore, to single out individual interaction type contributions, we compare the dimers without and with the Ag(111) substrate, and we omit (pure PBE calculations) or include vdW interactions intentionally. The latter is done by employing a pairwise TS vdW model[36] and also the more sophisticated MBD method.[38]

However, to justify a comparison between the experiment and theory, we first have to make sure that the observed assemblies correspond to equilibrium structures, that is, they are not kinetically frustrated.

As shown in Figure S21a, the kinetic energy of 6P deposited onto substrates at ca. 70 K is sufficient for the molecules to align along the Ag[110] direction, thereby overcoming the rotational energy barriers associated with their very asymmetric shape. In addition, Figure S21b evidences that densely packed and ordered monolayers form once surface energy minimization acts as the driving force. This is further proof that the kinetic energy is indeed sufficient to find the energetic minimum. The 6P molecules that are shown in Figure 2 were deposited onto the substrate held at room temperature, additionally guaranteeing that no kinetic barriers influence the molecular self-assembly.

To see whether the stack-shifts of m-2F-6P and o-2F-6P assemblies correspond to their equilibrium state, we take a closer look at their long-range stacking direction. Figure 6a,b depicts m-2F-6P and o-2F-6P on Ag(111), respectively, with higher coverage than those shown in Figures 3 and 4. As mentioned above, the stacking directions along the supramolecular chains (indicated by the red arrows and white dashed lines) clearly deviate from assumed stacking perpendicular to the long molecular axes (represented by the blue and black arrows in the same figures). This deviation is a macroscopic manifestation of different stack-shift distributions at the two sides of a given molecule. This can be attributed to the fact that the long molecular axes and the [211] ([110]) direction enclose an angle of ca. ±6° (±24°). For the molecules to the left and right of a given molecule in the row (L and R, respectively; see Figure 6c for definition), this results in different epitaxial registries for assumed identical stack-shifts. Thus, the energetic landscapes on the two sides of a given molecule are slightly different, causing L and R molecules to attach with different average stack-shifts. Being rotated by 180°, the inverted consideration applies for the following
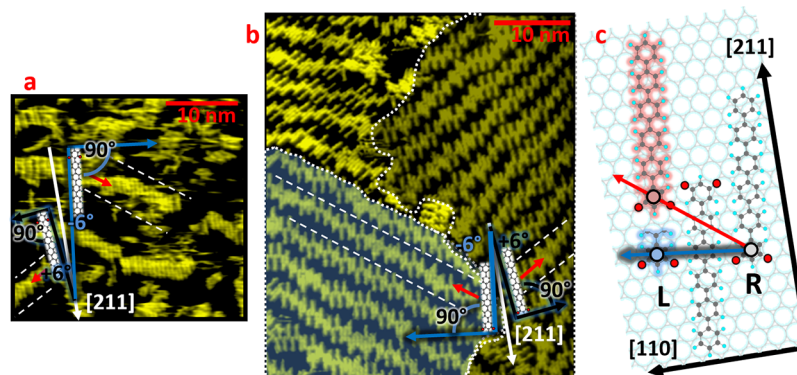

Figure 6. Oriented supramolecular chains at higher coverage. (a,b) Large-area STM images that show self-assembled rows of o-2F-6P and m-2F-6P molecules on Ag(111), respectively. The blue and black lines identify the two surface enantiomers [a: V = 1 V, I = 0.3 nA, 29.8 nm × 28.4 nm scan; b: V = 1 V, I = 0.3 nA, 47 nm × 45 nm scan]. (c) Illustration (for m-2F-6P) showing nonequal epitaxial registries for the molecule on the left (L) and right (R) of a given molecule.
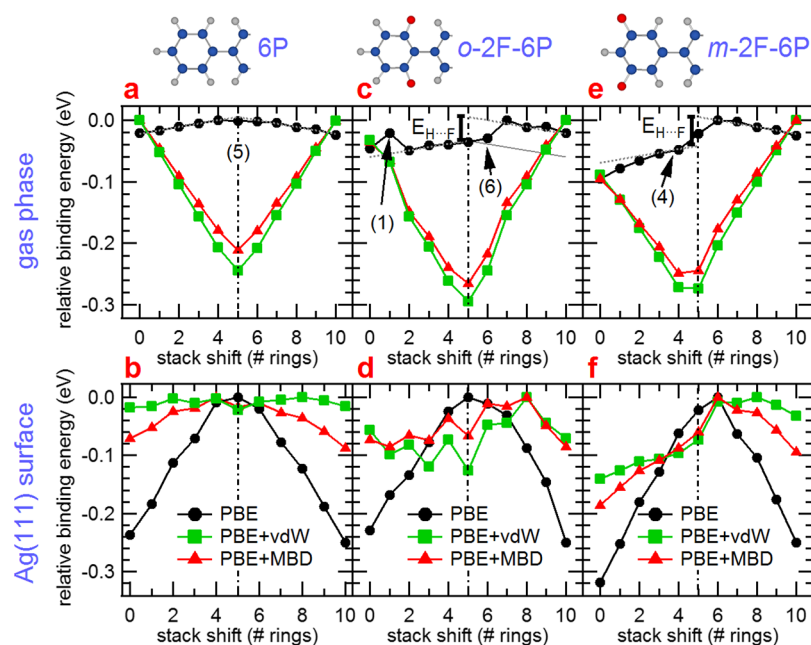
Figure 7. Calculated dimer binding energies. (a) Binding energy vs lateral displacement (stack-shift; see Figure 5 for nomenclature) for gas-phase 6P dimer arrangements calculated using PBE (black circles), PBE + vdW (green squares), and PBE + MBD (red triangles) methods. The binding energy of each dimer is plotted with respect to the energy of the least stable structure. (b) Same as (a) but with dimer structures on Ag(111) surface. (c,d) Same as (a,b), respectively, but for *o*-2F-6P dimer arrangements. (e,f) Same as (a,b), respectively, but for *m*-2F-6P dimer arrangements. The error bars of the calculations themselves are ca. 3 meV, that is, roughly represented by the symbol size. However, the adsorption geometries can only be approximately accounted for in these calculations, adding another uncertainty of ca. 20 meV upon including the Ag(111) surface.

molecules within a row, in turn giving rise to the observed finite angle between the stacking direction and the long molecular axes. By contrast, a long-range stacking direction perpendicular to the molecular axes would be found for random attachment of molecules expected for kinetically frustrated molecular arrangements.

For *m*-2F-6P, depositions with the substrate either at ca. 70 K or at room temperature, as well as postdeposition annealing, all resulted in the same stack-shift distribution. This shows that all observed structures have equally reached their equilibrium configuration, and that the variation in the stack-shift along the supramolecular chains stems from the entropic disorder. Long-range oriented supramolecular chains with entropic disorder were also observed for *o*-2F-6P deposited onto Ag(111) held at room temperature, which is evidence for an equilibrium situation in this case also. *m*-2F-6P primarily exhibits stack-shifts for L and R in the range of (0) to (5) and (0) to (2), respectively, whereas for most *o*-2F-6P molecules, the respective stack-shifts ranges are (4)−(6) and (2)−(5), resulting in similar stacking directions in the two cases.

We now turn toward the calculated energy curves as a function of stack-shift. The results for 6P dimers are summarized in Figure 7a,b, with the binding energy plotted with respect to the energy of the least stable structure. In the gas phase, PBE favors the least lateral proximity of the molecules, represented by structures (0) and (10) in our model. This is due to Pauli repulsion, giving rise to the repulsive part of the intramolecular interaction potential, which is included in the standard PBE calculations. The inclusion of attractive intermolecular interactions via parameterized vdW forces and many-body dispersion in more realistic functionals (PBE + vdW and PBE + MBD, respectively) expectedly changes this trend and returns the side-by-side configuration

(5) as the most stable arrangement of 6P in the gas phase. The dimer binding energy scales with the number of laterally overlapping benzene rings and is estimated from the slope of each branch of the V-shaped relations in Figure 7a as ca. 45 meV per ring pair.

The situation changes radically upon including the Ag(111) surface. A small but finite electron transfer of 0.04 electrons from the metal to each 6P molecule induces a dipolar electrostatic density distribution between the molecule and the surface. The charge transfer was computed using the Hirshfeld partitioning of the electron density.[47] The transferred charge is the sum of the atomic charges on the molecule (or equivalently the surface) computed from the self-consistent electron density of the combined molecule/surface system. Consequently, the interaction of equally oriented dipoles of neighboring molecules gives rise to repulsion, as expressed by the strong inverted V-shape of the PBE relation in Figure 7b. Note that the charge is distributed throughout the molecule in the former lowest unoccupied molecular orbital, meaning that a point dipole model will not represent the repulsion adequately. From the slope in Figure 7b, we estimate the repulsive energy per laterally overlapping benzene ring pair to be ca. 58 meV. Including polarization and dispersion via PBE + vdW and PBE + MBD calculations reduces the intermolecular repulsion significantly. As seen from the experimental observation (Figure 2), molecular aggregation is still energetically not favored. Consistently, the interaction energies for on-surface 6P dimer formation in the PBE + MBD calculations are positive (cf. Table S2), pointing to a net destabilizing intermolecular interaction. In addition, at low coverages beyond-dipole correlation effects could provide an additional mechanism for repulsive interactions.[48] Similar cases of intermolecular repulsion were observed previously in several

studies including 6P on Cu(111) and *para*-quaterphenyl on Au(111)[19,49−56] and also the transition from individually adsorbed molecules at low coverage to densely packed assemblies at higher coverage.[49−56] Dense packing goes in hand with the reduced charge transfer per molecule, but becomes energetically favorable because of the minimization of the surface energy as molecules cover the metal surface (compare, e.g., refs[57,58]).

The same type of dimer-based modeling was performed for *o*- and *m*-2F-6P (Figure 7c−f). For both molecules, we find the same small electron transfer from the metal, implying that the repulsion of surface-normal dipoles persists, but we can now revert to the details of attractive interactions that allow for aggregate formation in the low-coverage regime as seen in the experiment. First of all, from the dimer binding energy dependence on stack-shift obtained from PBE in the gas phase, we can retrieve the strength of the H···F bond for our fluoroaromatics. From Figure 7c, we observe linear trends for *o*-2F-6P when going from structure (2) to (6) and from (7) to (10). The slopes of these trends are representative of the Pauli repulsion per laterally overlapping benzene rings and equal to those found for 6P in Figure 7a. Notably, there is an offset $E_{H···F}$ between the two lines when going from configuration (6) to (7), which coincides with either having the possibility of forming two H···F bonds per dimer or none. This means that hydrogen bonds contribute significantly also for configuration (6) that has the fluorine-bearing terminal benzene ring without a direct neighboring benzene ring, rationalizing the observation of this configuration despite a seemingly less perfect lateral overlap. A deviation from maximum hydrogen bond strength for this configuration is apparent from the difference between the corresponding binding energy and that of configuration (4), as visualized in Figure 7c by means of the solid line. Conversely, configuration (0) lacks maximum stabilization because it only features hydrogen bonding to the neighboring ring but does not benefit from an additional interaction with a second ring. Fully analogous behavior is observed for *m*-2F-6P; only the configurations where the transition from no to full hydrogen bond stabilization occurs are shifted to (4)/(6), whereas in this case, configuration (5) is in between in terms of full H···F bond formation capability. Apparently, the intermolecular bonds formed by the fluorine atoms feature contributions from more than one hydrogen atom and involve up to two rings. In addition, Arras et al. concluded for an equivalent atomic configuration that the proton acceptor interacts with the whole benzene ring, including important contributions from the C−H groups on the far side.[59] This means that the interaction at hand exceeds the local character of a typical hydrogen bond.

It is worthwhile noting that $E_{H···F}$ is identical for *m*-2F-6P and *o*-2F-6P, whereas for any assumed effect of the molecular dipole via dipole-induced dipole interaction, the step size should relate to the rather different dipole moments of the two molecules.

Although here, only stack-shifts by integer benzene rings were considered to warrant comparability between the configurations, maximum stabilization could occur for other shift values. A detailed calculation of noninteger stack-shifts (see Figure S1) allows us to estimate the binding energy per H···F bond of up to 30 meV (25 meV for integer-only stack-shifts) for the molecules considered here. The atomic configurations that correspond to the minima in the binding energy curve—with the fluorine atom being located in between

two hydrogen atoms of a benzene ring or in between two phenyl groups—agree with those found for 6P-dicarbonitrile/Ag(111)[60] and also the experimentally observed stack-shifts (Figures 3b and 4b).

Inspection of Figure 7c reveals that configuration (1) for *o*-2F-6P is destabilized in energy compared to the straight line. This is attributed to the strong repulsion of two highly polar C−F bonds facing each other. For *m*-2F-6P, the slope of the left branch (see Figure 7e) is found to be steeper than for the other two molecules. We believe that this is due to the two intramolecular dipoles coming into an energy-minimized antiparallel arrangement, leading to additional stabilization of the (0) and (1) configurations. We note that an apparent contribution to the dimer structure from intramolecular dipole interactions is missing for *o*-2F-6P, which we ascribe to the smaller overall dipole moment and the fact that the electric potential distribution in the near field (the one relevant for two molecules in proximity), as shown in Figure 1b, deviates strongly from a simple dipolar pattern.

By including vdW interactions via PBE + vdW and PBE + MBD calculations (Figure 7c,e), the trends for gas-phase dimers change toward the V-shape already observed for 6P, with an energy minimum at or near configuration (5). As this configuration was not observed in the experiment for *o*- and *m*-2F-6P, the metal substrate must play a key role. In pure PBE calculations, the surface-normal dipole−dipole repulsion, induced by the metal-to-molecule electron transfer, dominates and results in the distinct reversed V-shape (Figure 7d,f). For *o*-2F-6P, including the vdW and MBD interactions causes a range of configurations becoming very similar in energy. The reduced structural symmetry upon including the substrate gives rise to more pronounced fluctuations in the calculated energy curves. When we bear in mind that noninteger stack-shifts can facilitate stronger hydrogen bonds, we see that configurations (2) to (6) are plausible, which we indeed find in the experiment (Figure 3). Apparently, the formation of H···F bonds, in combination with the polarization and dispersion interactions brought about by the substantial lateral overlap of neighboring molecules, is sufficient to overcome the charge transfer-induced dipole repulsion, and aggregation of *o*-2F-6P molecules to rows with small stack-shifts can occur at a very low absolute substrate coverage. The fact that the calculations reveal no clear energy minimum is reflected in the observation of several different stack-shifts in Figure 3.

Configurations (0) and (1) are not found for *o*-2F-6P, as the H···F bonds are weak or even antibonding. Configurations without H···F bonds are unstable as well. As already discussed for the gas-phase dimers above, the interaction of intramolecular dipoles (i.e., in-plane) does not contribute notably to the assembly energy.

For *m*-2F-6P, the energy minimum is found for configuration (0) (see Figure 7f). As this is the configuration we also find in the experiment (Figure 4), we conclude that here the H···F bonds and the (comparably smaller) intramolecular dipole interaction (crudely estimated in a point dipole model to be 11 meV) are overall stabilizing, whereas the small lateral overlap between direct neighbor molecules reduces polarization- and dispersion-related stabilization. However, this seems compensated by the wider separation of destabilizing surface-normal dipoles in the configurations with large stack-shifts. Like for *o*-2F-6P, the relatively flat energy curves for calculations that assume *m*-2F-6P molecules aligned with [110] will be slightly altered by the actual mismatch of long

molecular axes and the Ag high-symmetry directions. This can explain why configuration (0) dominates predominantly on one side of a given m-2F-6P molecule, whereas its other side sometimes exhibits smaller stack-shifts. From a comparison of the binding energies of configurations (0) and (10) for m-2F-6P, we can estimate the combined dimer stabilizing energy due to two H···F bonds and in-plane dipole arrangement to be ca. 100 meV.

Similar energetic considerations apply for the appearance of the canted arrangements found for m-2F-6P, typically at the end of rows (Figure 4c). While not possible for o-2F-6P with its fluorine atoms in ortho position, the meta position of m-2F-6P's fluorine atoms allows the formation of H···F bonds between two m-2F-6P molecules also when the molecules "dock" with their heads while their long molecular axes form an angle of ≈60° with neighboring molecules (Figure 4c). This is a supramolecular building block (synthon) that was also found for 1,4-difluorobenzene, 1,3,5-trifluorobenzene, and 1,2,3,4-tetrafluorobenzene crystals.[61,62] Noteworthy, several docking arrangements appear similarly stable. This is apparent in Figure 4a from the different configurations at the two ends of the molecular row. In addition, manipulation with the STM tip induces the docking directions of molecules in canted arrangements to change repeatedly through a variety of configurations, as reported in Figure S23. This corresponds to a wide range of possible C−F···H−C angles that all result in hydrogen bond formation, consistent with the rather flat interaction potential map between proton acceptors and organic rings found in ref 59, and evidence that employing this geometric parameter for the identification of hydrogen bonds, as typically done in crystal structure analysis,[21−24] might not be appropriate for the H···F connected structures investigated here. For comparison, we also studied m-4F-6P, a symmetric congener of m-2F-6P, in the solid state by means of single-crystal X-ray analysis, where the existence of significant classic H···F bonds can be observed via short to medium intermolecular H···F contacts[61,62] (2.43−2.67 Å with angles 143−175°, cf. Table S3), leaving little doubt that these weak interactions govern the overall structural alignment, at least to some extent.

CONCLUSIONS

In summary, we obtained detailed insight into the intricate interplay of attractive and repulsive interactions that govern the self-assembly of molecules on a metal surface. Three structurally very similar conjugated molecules, that is, 6P and the analogues o-2F-6P and m-2F-6P with two fluorine atoms each, showed vastly different assembly phenomenology on Ag(111). A satisfactory explanation of the experimental observations based on known molecular properties, such as intramolecular dipole moment, and presumed intermolecular interactions, such as H···F bond formation, could not be obtained, as a hierarchical ordering of all involved interactions and their coaction is not reliably possible. Only by employing a range of DFT methods, we could understand that the strongest repulsive component in all three systems is the Coulombic repulsion resulting from the minute electron transfer from the metal to each molecule. Of comparable magnitude but of attractive character are intermolecular vdW interactions for densely packed molecules, that is, polarization and dispersion. Yet, for 6P, repulsion dominates and only isolated adsorbed molecules persist in the low-coverage regime, and assembled structures only form close to monolayer coverage. For the

partially fluorinated molecules, the H···F bond formation propensity turns out as the key factor enabling the formation of stable nanoscale molecular assemblies at very low absolute molecular coverage. Because of the small magnitude of the dipole moment of o-2F-6P (1.1 D) and the pronounced deviation from a dipole charge pattern in the near field, the influence of this intramolecular dipole on the assembly structure was found to be negligible. By contrast, for m-2F-6P, the charge pattern causing the intramolecular dipole (2.2 D) facilitates a small stabilizing dipole−dipole interaction. In conjunction with geometry-optimized H···F bonds between m-2F-6P molecules that contribute a binding energy of up to 30 meV per bond, zipper-like rows form. o-2F-6P rows that approach a zipper-like configuration, however, suffer from destabilized hydrogen bonds because of the Coulomb repulsion between the fluorine atoms in the ortho configuration. Jointly with the absence of a significantly stabilizing dipole−dipole interaction, this explains the dense packing observed for o-2F-6P. Only with this detailed understanding of all interactions and their interplay, it becomes feasible to design molecules for achieving targeted self-assembly structures, based on weak interactions only. Importantly, we illustrate ways how to circumvent dominating repulsive interactions at very low molecular surface coverage. This enables the realization of individual and stable nanoscale molecular assemblies and their study, without the need to approach monolayer coverage, which could substantially alter the obtained structure. Furthermore, the insight provided here helps in understanding how fluorine substitution in conjugated molecules and polymers contributes to thin film and bulk structures, which, in turn, will enable realizing organic electronic materials with superior optical and charge-transport properties for electronic and optoelectronic applications.

ASSOCIATED CONTENT

Ⓢ Supporting Information

The Supporting Information is available free of charge on the ACS Publications website at DOI: 10.1021/acs.jpcc.8b03398.

First-principles electronic structure calculations: additional calculations for dimers with noninteger stack-shift, visualization of on-surface structures, relaxed versus single-point calculations, and interaction energies for 6P dimer formation on Ag(111); synthetic and analytical methods: ^{1}H and ^{13}C NMR spectra of intermediates and precursors as well as infrared spectra of the final compounds and 6P; and additional scanning tunneling data: molecular arrangement of 6P in the monolayer regime, detailed discussion of o-2F-6P and m-2F-6P arrangements, scanning tunneling spectroscopy results for m-2F-6P, manipulation of a canted arrangement with the STM tip, line profiles for m-2F-6P, and experimental details and results of the single-crystal X-ray analysis of m-4F-6P (PDF)

Crystal structure of m-4F-6P (CIF)

AUTHOR INFORMATION

Corresponding Authors
*E-mail: norbert.koch@physik.hu-berlin.de (N.K.).
*E-mail: hla@ohio.edu (S.-W.H.).

ORCID Ⓘ
Fairoja Cheenicode Kabeer: 0000-0003-1450-0615
Stefan Hecht: 0000-0002-6124-0222

Alexandre Tkatchenko: 0000-0002-1012-4854
Norbert Koch: 0000-0002-6042-6447

Author Contributions

■ REFERENCES

(1) Whitesides, G. M.; Grzybowski, B. Self-Assembly at All Scales. *Science* **2002**, *295*, 2418−2421.

(2) Packwood, D. M.; Han, P.; Hitosugi, T. Chemical and Entropic Control on the Molecular Self-Assembly Process. *Nat. Commun.* **2017**, *8*, 14463.

(3) MacLeod, J. M.; Rosei, F. Molecular Self-Assembly on Graphene. *Small* **2014**, *10*, 1038−1049.

(4) Lehn, J.-M. Perspectives in Supramolecular Chemistry-From Molecular Recognition towards Molecular Information Processing and Self-Organization. *Angew. Chem., Int. Ed.* **1990**, *29*, 1304−1319.

(5) Palmer, L. C.; Stupp, S. I. Molecular Self-Assembly Into One-Dimensional Nanostructures. *Acc. Chem. Res.* **2008**, *41*, 1674−1684.

(6) *Supramolecular Materials for Opto-Electronics*; Koch, N., Ed.; Royal Society of Chemistry, 2015; pp 53−118, ISBN 978-1-84973-826-2.

(7) Wang, A.; Shi, W.; Huang, J.; Yan, Y. Adaptive Soft Molecular Self-Assemblies. *Soft Matter* **2016**, *12*, 337−357.

(8) Baber, A. E.; Jensen, S. C.; Sykes, E. C. H. Dipole-Driven Ferroelectric Assembly of Styrene on Au{111}. *J. Am. Chem. Soc.* **2007**, *129*, 6368−6369.

(9) Niederhausen, J.; Kersell, H. R.; Christodoulou, C.; Heimel, G.; Wonneberger, H.; Müllen, K.; Rabe, J. P.; Hla, S.-W.; Koch, N. Monolayer Phases of a Dipolar Perylene Derivative on Au(111) and Surface Potential Build-Up in Multilayers. *Langmuir* **2016**, *32*, 3587−3600.

(10) Slater, A. G.; Perdigão, L. M. A.; Beton, P. H.; Champness, N. R. Surface-Based Supramolecular Chemistry Using Hydrogen Bonds. *Acc. Chem. Res.* **2014**, *47*, 3417−3427.

(11) Barth, J. V.; Weckesser, J.; Cai, C.; Günter, P.; Bürgi, L.; Jeandupeux, O.; Kern, K. Building Supramolecular Nanostructures at Surfaces by Hydrogen Bonding. *Angew. Chem., Int. Ed.* **2000**, *39*, 1230−1234.

(12) Liu, W.; Tkatchenko, A.; Scheffler, M. Modeling Adsorption and Reactions of Organic Molecules at Metal Surfaces. *Acc. Chem. Res.* **2014**, *47*, 3369−3377.

(13) Maurer, R. J.; Ruiz, V. G.; Camarillo-Cisneros, J.; Liu, W.; Ferri, N.; Reuter, K.; Tkatchenko, A. Adsorption Structures and Energetics of Molecules on Metal Surfaces: Bridging experiment and theory. *Prog. Surf. Sci.* **2016**, *91*, 72−100.

(14) Wang, Y. Z.; Sun, R. G.; Meghdadi, F.; Leising, G.; Epstein, A. J. Multicolor Multilayer Light-Emitting Devices Based on Pyridine-Containing Conjugated Polymers and para-Sexiphenyl Oligomer. *Appl. Phys. Lett.* **1999**, *74*, 3613.

(15) Simbrunner, C. Epitaxial Growth of Sexi-Thiophene and para-Hexaphenyl and its Implications for the Fabrication of Self-Assembled Lasing Nano-Fibres. *Semicond. Sci. Technol.* **2013**, *28*, 053001.

(16) Koller, G.; Berkebile, S.; Oehzelt, M.; Puschnig, P.; Ambrosch-Draxl, C.; Netzer, F. P.; Ramsey, M. G. Intra- and Intermolecular Band Dispersion in an Organic Crystal. *Science* **2007**, *317*, 351−355.

(17) Hla, S.-W.; Braun, K.-F.; Wassermann, B.; Rieder, K.-H. Controlled Low-Temperature Molecular Manipulation of Sexiphenyl Molecules on Ag(111) Using Scanning Tunneling Microscopy. *Phys. Rev. Lett.* **2004**, *93*, 208302.

(18) Braun, K.-F.; Hla, S.-W. Probing the Conformation of Physisorbed Molecules at the Atomic Scale Using STM Manipulation. *Nano Lett.* **2005**, *5*, 73−76.

(19) Oehzelt, M.; Grill, L.; Berkebile, S.; Koller, G.; Netzer, F. P.; Ramsey, M. G. The Molecular Orientation of para-Sexiphenyl on Cu(110) and Cu(110) p(2×1)O. *ChemPhysChem* **2007**, *8*, 1707−1712.

(20) Chen, W.; Zhang, H. L.; Huang, H.; Chen, L.; Wee, A. T. S. Self-Assembled Organic Donor/Acceptor Nanojunction Arrays. *Appl. Phys. Lett.* **2008**, *92*, 193301.

(21) Desiraju, G. R. Hydrogen Bridges in Crystal Engineering: Interactions without Borders. *Acc. Chem. Res.* **2002**, *35*, 565−573.

(22) Dunitz, J. D.; Taylor, R. Organic Fluorine Hardly Ever Accepts Hydrogen Bonds. *Chem.—Eur. J.* **1997**, *3*, 89−98.

(23) Shimoni, L.; Glusker, J. P. The Geometry of Intermolecular Interactions in Some Crystalline Fluorine-Containing Organic Compounds. *Struct. Chem.* **1994**, *5*, 383−397.

(24) Howard, J. A. K.; Hoy, V. J.; O'Hagan, D.; Smith, G. T. How Good is Fluorine as a Hydrogen Bond Acceptor? *Tetrahedron* **1996**, *52*, 12613−12622.

(25) de Oteyza, D. G.; Silanes, I.; Ruiz-Osés, M.; Barrena, E.; Doyle, B. P.; Arnau, A.; Dosch, H.; Wakayama, Y.; Ortega, J. E. Balancing Intermolecular and Molecule-Substrate Interactions in Supramolecular Assemblies. *Adv. Funct. Mater.* **2009**, *19*, 259−264.

(26) El-Sayed, A.; Mowbray, D. J.; García-Lastra, J. M.; Rogero, C.; Goiri, E.; Borghetti, P.; Turak, A.; Doyle, B. P.; Dell'Angela, M.; Floreano, L.; et al. Supramolecular Environment-Dependent Electronic Properties of Metal-Organic Interfaces. *J. Phys. Chem. C* **2012**, *116*, 4780−4785.

(27) Sparenberg, M.; Zykov, A.; Beyer, P.; Pithan, L.; Weber, C.; Garmshausen, Y.; Carlà, F.; Hecht, S.; Blumstengel, S.; Henneberger, F.; et al. Controlling the Growth Mode of para-Sexiphenyl (6P) on ZnO by Partial Fluorination. *Phys. Chem. Chem. Phys.* **2014**, *16*, 26084−26093.

(28) Nielsen, C. B.; White, A. J. P.; McCulloch, I. Effect of Fluorination of 2,1,3-Benzothiadiazole. *J. Org. Chem.* **2015**, *80*, 5045−5048.

(29) Fischer, F. S. U.; Kayunkid, N.; Trefz, D.; Ludwigs, S.; Brinkmann, M. Structural Models of Poly(cyclopentadithiophene-alt-benzothiadiazole) with Branched Side Chains: Impact of a Single Fluorine Atom on the Crystal Structure and Polymorphism of a Conjugated Polymer. *Macromolecules* **2015**, *48*, 3974−3982.

(30) Do, K.; Saleem, Q.; Ravva, M. K.; Cruciani, F.; Kan, Z.; Wolf, J.; Hansen, M. R.; Beaujuge, P. M.; Brédas, J.-L. Impact of Fluorine Substituents on π-Conjugated Polymer Main-Chain Conformations, Packing, and Electronic Couplings. *Adv. Mater.* **2016**, *28*, 8197−8205.

(31) Li, W.; Albrecht, S.; Yang, L.; Roland, S.; Tumbleston, J. R.; McAfee, T.; Yan, L.; Kelly, M. A.; Ade, H.; Neher, D.; et al. Mobility-Controlled Performance of Thick Solar Cells Based on Fluorinated Copolymers. *J. Am. Chem. Soc.* **2014**, *136*, 15566−15576.

(32) Fei, Z.; Eisner, F. D.; Jiao, X.; Azzouzi, M.; Röhr, J. A.; Han, Y.; Shahid, M.; Chesman, A. S. R.; Easton, C. D.; McNeill, C. R.; et al. An Alkylated Indacenodithieno[3,2-b]thiophene-Based Nonfullerene Ac-

ceptor with High Crystallinity Exhibiting Single Junction Solar Cell Efficiencies Greater than 13% with Low Voltage Losses. *Adv. Mater.* **2018**, *30*, 1705209.

(33) Garmshausen, Y.; Schwarz, J.; Hildebrandt, J.; Kobin, B.; Pätzel, M.; Hecht, S. Making Nonsymmetrical Bricks: Synthesis of Insoluble Dipolar Sexiphenyls. *Org. Lett.* **2014**, *16*, 2838−2841.

(34) Hla, S.-W. Scanning Tunneling Microscopy Single Atom/ Molecule Manipulation and Its Application to Nanoscience and Technology. *J. Vac. Sci. Technol., B: Microelectron. Nanometer Struct.– Process., Meas., Phenom.* **2005**, *23*, 1351−1360.

(35) Blum, V.; Gehrke, R.; Hanke, F.; Havu, P.; Havu, V.; Ren, X.; Reuter, K.; Scheffler, M. Ab Initio Molecular Simulations with Numeric Atom-Centered Orbitals. *Comput. Phys. Commun.* **2009**, *180*, 2175−2196.

(36) Tkatchenko, A.; Scheffler, M. Accurate Molecular Van Der Waals Interactions from Ground-State Electron Density and Free-Atom Reference Data. *Phys. Rev. Lett.* **2009**, *102*, 073005.

(37) Ruiz, V. G.; Liu, W.; Zojer, E.; Scheffler, M.; Tkatchenko, A. Density-Functional Theory with Screened van der Waals Interactions for the Modeling of Hybrid Inorganic-Organic Systems. *Phys. Rev. Lett.* **2012**, *108*, 146103.

(38) Tkatchenko, A.; DiStasio, R. A., Jr.; Car, R.; Scheffler, M. Accurate and Efficient Method for Many-Body van der Waals Interactions. *Phys. Rev. Lett.* **2012**, *108*, 236402.

(39) Lifshitz, E. M. The Theory of Molecular Attractive Forces Between Solids. *Sov. Phys.—JETP* **1956**, *2*, 73−83.

(40) Schatschneider, B.; Liang, J.-J.; Reilly, A. M.; Marom, N.; Zhang, G.-X.; Tkatchenko, A. Electrodynamic Response and Stability of Molecular Crystals. *Phys. Rev. B: Condens. Matter Mater. Phys.* **2013**, *87*, 060104.

(41) Perdew, J. P.; Burke, K.; Ernzerhof, M. Generalized Gradient Approximation Made Simple. *Phys. Rev. Lett.* **1996**, *77*, 3865−3868.

(42) van Lenthe, E.; Baerends, E. J.; Snijders, J. G. Relativistic Total Energy Using Regular Approximations. *J. Chem. Phys.* **1994**, *101*, 9783−9792.

(43) Monkhorst, H. J.; Pack, J. D. Special Points for Brillouin-Zone Integrations. *Phys. Rev. B: Solid State* **1976**, *13*, 5188−5192.

(44) Liu, W.; Ruiz, V. G.; Zhang, G.-X.; Santra, B.; Ren, X.; Scheffler, M.; Tkatchenko, A. Structure and Energetics of Benzene Adsorbed on Transition-Metal Surfaces: Density-Functional Theory with van der Waals Interactions Including Collective Substrate Response. *New J. Phys.* **2013**, *15*, 053046.

(45) Liu, W.; Maaß, F.; Willenbockel, M.; Bronner, C.; Schulze, M.; Soubatch, S.; Tautz, F. S.; Tegeder, P.; Tkatchenko, A. Quantitative Prediction of Molecular Adsorption: Structure and Binding of Benzene on Coinage Metals. *Phys. Rev. Lett.* **2015**, *115*, 036104.

(46) *Charge-Carrier Mobility in Organic Crystals*; Farchioni, R., Grosso, G., Eds.; Springer Berlin Heidelberg, 2001; pp 283−326.

(47) Hirshfeld, F. L. Bonded-Atom Fragments for Describing Molecular Charge Densities. *Theor. Chim. Acta* **1977**, *44*, 129−138.

(48) Sadhukhan, M.; Tkatchenko, A. Long-Range Repulsion Between Spatially Confined van der Waals Dimers. *Phys. Rev. Lett.* **2017**, *118*, 210402.

(49) Müllegger, S.; Salzmann, I.; Resel, R.; Hlawacek, G.; Teichert, C.; Winkler, A. Growth Kinetics, Structure, and Morphology of para-Quaterphenyl Thin Films on Gold(111). *J. Chem. Phys.* **2004**, *121*, 2272−2277.

(50) Lukas, S.; Witte, G.; Wöll, C. Novel Mechanism for Molecular Self-Assembly on Metal Substrates: Unidirectional Rows of Pentacene on Cu(110) Produced by a Substrate-Mediated Repulsion. *Phys. Rev. Lett.* **2001**, *88*, 028301.

(51) Stadler, C.; Hansen, S.; Kröger, I.; Kumpf, C.; Umbach, E. Tuning Intermolecular Interaction in Long-Range-Ordered Submonolayer Organic Films. *Nat. Phys.* **2009**, *5*, 153−158.

(52) Duhm, S.; Bürker, C.; Niederhausen, J.; Salzmann, I.; Hosokai, T.; Duvernay, J.; Kera, S.; Schreiber, F.; Koch, N.; Ueno, N.; et al. Pentacene on Ag(111): Correlation of Bonding Distance with Intermolecular Interaction and Order. *ACS Appl. Mater. Interfaces* **2013**, *5*, 9377−9381.

(53) Wagner, C.; Kasemann, D.; Golnik, C.; Forker, R.; Esslinger, M.; Müllen, K.; Fritz, T. Repulsion between Molecules on a Metal: Monolayers and Submonolayers of hexa-peri-Hexabenzocoronene on Au(111). *Phys. Rev. B: Condens. Matter Mater. Phys.* **2010**, *81*, 035423.

(54) Seidel, C.; Ellerbrake, R.; Gross, L.; Fuchs, H. Structural Transitions of Perylene and Coronene on Silver and Gold Surfaces: A Molecular-Beam Epitaxy LEED Study. *Phys. Rev. B: Condens. Matter Mater. Phys.* **2001**, *64*, 195418.

(55) Thussing, S.; Jakob, P. Structural and Vibrational Properties of CuPc/Ag(111) Ultrathin Films. *J. Phys. Chem. C* **2016**, *120*, 9904−9913.

(56) Song, Z.; Schultz, T.; Ding, Z.; Lei, B.; Han, C.; Amsalem, P.; Lin, T.; Chi, D.; Wong, S. L.; Zheng, Y. J.; et al. Electronic Properties of a 1D Intrinsic/p-Doped Heterojunction in a 2D Transition Metal Dichalcogenide Semiconductor. *ACS Nano* **2017**, *11*, 9128−9135.

(57) Tyson, W. R.; Miller, W. A. Surface Free Energies of Solid Metals: Estimation from Liquid Surface Tension Measurements. *Surf. Sci.* **1977**, *62*, 267−276.

(58) Li, R.; Zhang, X.; Dong, H.; Li, Q.; Shuai, Z.; Hu, W. Gibbs-Curie-Wulff Theorem in Organic Materials: A Case Study on the Relationship between Surface Energy and Crystal Growth. *Adv. Mater.* **2016**, *28*, 1697−1702.

(59) Arras, E.; Seitsonen, A. P.; Klappenberger, F.; Barth, J. V. Nature of the Attractive Interaction between Proton Acceptors and Organic Ring Systems. *Phys. Chem. Chem. Phys.* **2012**, *14*, 15995−16001.

(60) Palma, C.-A.; Björk, J.; Klappenberger, F.; Arras, E.; Kühne, D.; Stafström, S.; Barth, J. V. Visualization and Thermodynamic Encoding of Single-Molecule Partition Function Projections. *Nat. Commun.* **2015**, *6*, 6210.

(61) Thalladi, V. R.; Weiss, H.-C.; Bläser, D.; Boese, R.; Nangia, A.; Desiraju, G. R. C−H···F Interactions in the Crystal Structures of Some Fluorobenzenes. *J. Am. Chem. Soc.* **1998**, *120*, 8702−8710.

(62) Thakur, T. S.; Kirchner, M. T.; Bläser, D.; Boese, R.; Desiraju, G. R. C−H···F−C Hydrogen Bonding in 1,2,3,5-Tetrafluorobenzene and other Fluoroaromatic Compounds and the Crystal Structure of Alloxan Revisited. *CrystEngComm* **2010**, *12*, 2079−2085.